Marine and Petroleum Geology 131 (2021) 105153

Contents lists available at ScienceDirect

Marine and Petroleum Geology

journal homepage: www.elsevier.com/locate/marpetgeo

Research paper

Sedimentary environment constraints on the diagenetic evolution of clastic reservoirs: Examples from the Eocene "red-bed" and "gray-bed" in the Dongying Depression, China

Jian Wang [a,b,c,*], Yuhan Pang [a,b], Yingchang Cao [a,b,c,**], Jie Peng [a,b], Keyu Liu [a,b,d], Huimin Liu [e]

[a] Shandong Provincial Key Laboratory of Deep Oil & Gas, Qingdao, 266580, China
[b] China University of Petroleum (East China), Qingdao, 266580, China
[c] Laboratory for Marine Mineral Resources, Qingdao National Laboratory for Marine Science and Technology, Qingdao, 266071, China
[d] CSIRO Energy, 26 Dick Perry Drive, Kensington, WA, 6151, Australia
[e] Institute of the Shengli Oilfield, SINOPEC, Dongying, 257015, China

ARTICLE INFO

Keywords:
Diagenesis
Sedimentary environment
Red-bed sandstone
Gray-bed sandstone
Eocene
Dongying depression

ABSTRACT

The diagenetic characteristics and differences between the Eocene red-bed sandstone deposited in an arid environment and gray-bed sandstone deposited in a relatively humid environment were investigated systematically by an integrated analysis of petrography, X-ray diffraction, carbon and oxygen stable isotopes and fluid inclusion microthermometry. Strong eodiagenetic calcite and gypsum/anhydrite cementation occurred at the boundary of the Eocene red-bed sandstone, while the centre of the red-bed sandstone was characterized by relatively strong quartz dissolution and weak mesodiagenetic feldspar dissolution and ferro-carbonate cementation. Eodiagenetic calcite cementation at the boundary of the gray-bed sandstone and quartz dissolution were relatively weak, while the carbonate cemented zone at the boundary of the gray-bed sandstone was strengthened by mesodiagenetic ferro-carbonate cement. Relatively strong feldspar dissolution and ferro-carbonate cementation occurred in the centre of gray-bed sandstone beds. By comparing the diagenetic differences between the red-bed sandstones and gray-bed sandstones, it is shown that sedimentary environment had an obvious influence on reservoir diagenetic evolution and reservoir properties through influencing the chemical properties of connate water, the transformation rate and degree of clay minerals in interbedded mudstone, and the properties of diagenetic fluids during burial process.

1. Introduction

Diagenesis is an important controlling factor of clastic reservoir properties, contributing a decisive influence on the formation, preservation and destruction of pores in clastic reservoirs (Schmid et al., 2004; Al Gahtani, 2013; Nguyen et al., 2013; Wilson et al., 2013; Henares et al., 2014). Extensive research shows that diagenesis influences porosity and permeability of clastic reservoirs mainly through compaction, dissolution and cementation (Rossi et al., 2002; Morad et al., 2010; Wang et al., 2019a, b). At the same time, factors controlling reservoir diagenesis are discussed, mainly including petrological composition (Rossi et al., 2002; Karim et al., 2010; Wang et al., 2019a, b), temperature (Wang et al., 2018), formation pressure (Wilkinson et al., 1997; Osborne and Swarbrick, 1999), and fluid properties (Wang et al., 2016, 2018). Most studies on these controlling factors are focused on burial conditions and few scholars studied the diagenetic evolution from the perspective of the influence of the original sedimentary environment on diagenesis (Morad et al., 2010). Sedimentary environment can affect clastic reservoir diagenesis by influencing the detrital composition and the properties of early diagenetic fluids (Carvalho et al., 2014). The influence of different detrital composition on diagenesis has been discussed by many scholars (Alagarsamy et al., 2005; Henares et al., 2014), and the effects of which on compaction, cementation and dissolution have been systematically summarized (Caracciolo, 2020), indicating that the detrital composition play a foundational role in the diagenetic process of clastic reservoirs (Caracciolo, 2020). However, the influence of sedimentary environment on formation-fluid evolution and chemical diagenesis is rarely reported.

* Corresponding author. Shandong Provincial Key Laboratory of Deep Oil & Gas, Qingdao, 266580, China.
** Corresponding author. Shandong Provincial Key Laboratory of Deep Oil & Gas, Qingdao, 266580, China.
E-mail address: wangjian8601@upc.edu.cn (J. Wang).

https://doi.org/10.1016/j.marpetgeo.2021.105153
Received 6 September 2020; Received in revised form 15 May 2021; Accepted 17 May 2021
Available online 25 May 2021

Depositional environment controls connate water properties, and then determines the nature of connate water trapped between sediment particles, which directly affects the evolution characteristics of pore fluid and diagenesis of clastic rocks during the burial process (Carvalho et al., 2014). The differences of diagenetic evolution often determine the difference of formation mechanism of high-quality reservoirs, which is of great significance for understanding the development of high-quality clastic reservoirs in different sedimentary environments.

The fourth member of the Eocene Shahejie Formation (Es4) developed during the initial rift stage of the Dongying Depression with relatively stable tectonic conditions (Lampe et al., 2012). Abundant thin layer sandbodies were developed in the gentle slope belt of the Dongying Depression. During the depositional period of the lower Es4 (Es4x), widespread red thin layer sandstones interbedded with red mudstones (red bed) in the southern Dongying Depression were developed under an arid paleoclimate (Wang et al., 2015; Liu et al., 2017). During the depositional period of the upper Es4 (Es4s), gray thin layer sandstone-mudstone intervals (gray bed) in the southern Dongying Depression were developed under a relatively wet paleoclimatic condition (Jiang et al., 2011; Wang et al., 2019a, b). The two sets of strata are closely adjacent, and the burial processes were similar, which is an ideal area to study the influence of sedimentary environment on the diagenetic evolution of clastic reservoirs. In this study, we investigated the characteristics and differences of diagenesis between red-bed and gray-bed reservoirs in the Dongying Depression using an integrated petrology, mineralogy and geochemistry analysis to determine the

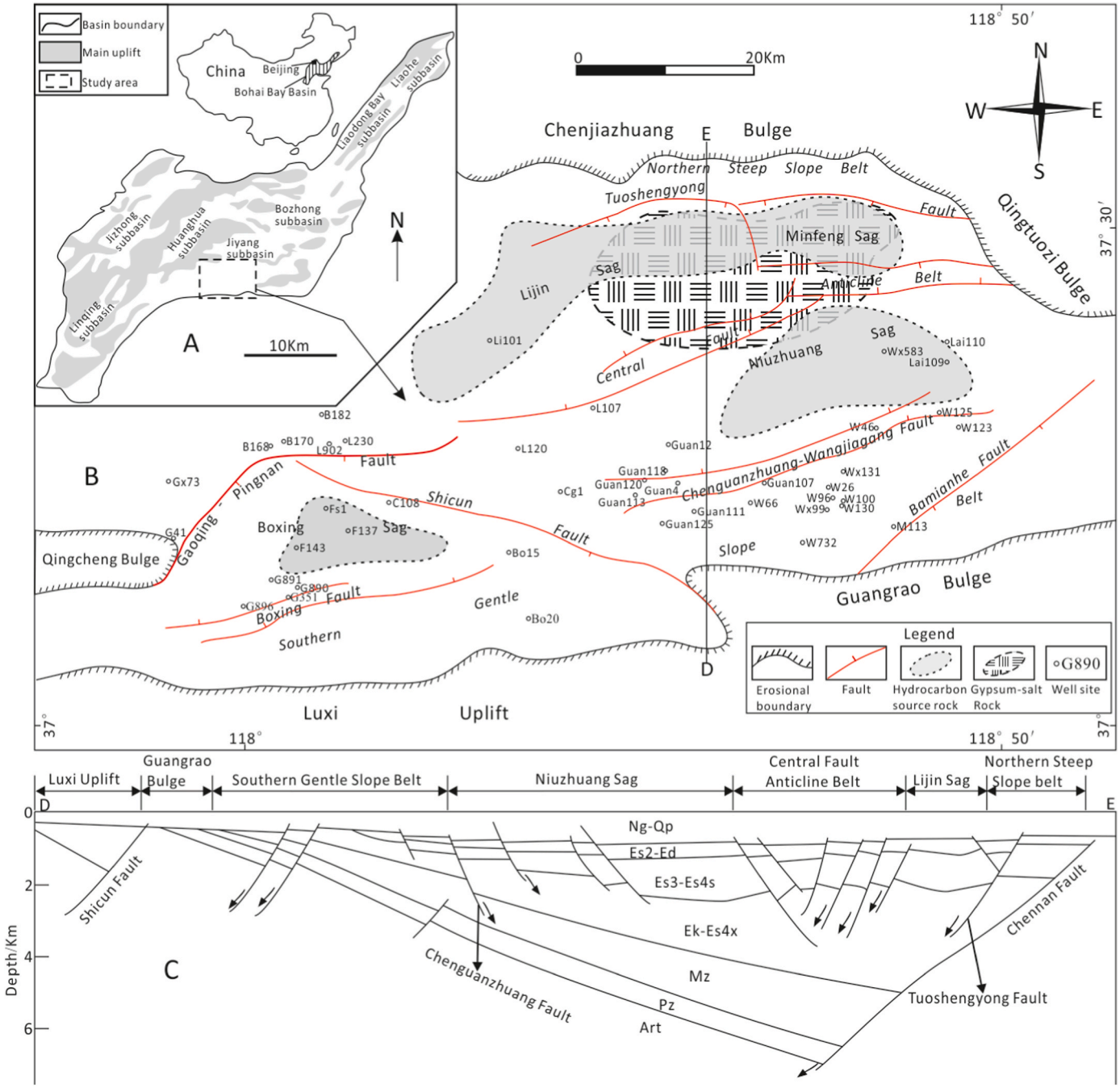

Fig. 1. (A) Location map showing subunits of the Bohai Bay Basin. (B) Gypsum-salt deposits and hydrocarbon source rock distribution, the locations of section DE, wells and main normal faults in the study area. (C) Cross section DE showing the different tectonic zones within the Dongying Depression.

controls of sedimentary environment on clastic reservoir diagenesis. The results can provide a basis and an example for similar situations in other basins.

2. Geological background

The Bohai Bay Basin is an important hydrocarbon producing basin in eastern China, covering an area of approximately 200,000 km^2. The basin is a complex rifted basin that formed in the Late Jurassic through to the early Tertiary on the basement of the North China platform. The tectonic evolution of the basin consists of a synrift stage (65.0–24.6 Ma) and postrift stage (24.6 Ma to present) (Lampe et al., 2012). The Bohai Bay Basin consists of several subbasins (Fig. 1A). The Dongying Depression is a secondary tectonic unit in the Jiyang Subbasin surrounded by the Qingtuozi Bulge in the east, Guangrao Bulge in the southeast, Luxi Uplift in the south, Gaoqing Bulge in the west and the Chenguangzhuang Bulge in the north (Fig. 1B).

The Dongying Depression was filled with Cenozoic sediments, consisting of the Paleogene Kongdian (Ek), Shahejie (Es), and Dongying (Ed) Formations, the Neogene Guantao (Ng) and Minghuazhen (Nm) Formations, and the Quaternary Pingyuan (Qp) Formation (Fig. 2). Influenced by the Himalayan movement, the development and evolution of the synrift basin experienced three stages: initial rift stage (Ek and fourth member of Es (Es4)), strong rift stage (third member of Es (Es3) and lower submember of the second member of Es (Es2x)) and atrophic rift stage (upper submember of the second member of Es (Es2s), first member of Es (Es1) and Ed). These three stages comprised the whole sedimentary filling process of the synrift stage of the Dongying Depression and formed a whole sedimentary cycle with the sequence from shore-shallow lacustrine facies to deep lacustrine facies and then to shore-shallow lacustrine facies.

Affected by the gentle paleogeomorphology and oscillatory lake level, the sandbodies in Es4 are thin (Wang et al., 2019a, b). During the depositional period of Es4x, affected by the arid paleoclimate, the salinity of the lake was relatively high. A widely distributed flood-prone delta developed in the southern gentle slope belt, and thick gypsum-salt beds were deposited in the centre of the lake (Wang et al., 2015). During the depositional period of Es4s, the paleoclimate gradually became wetter, the salinity of lake decreased, and a wide range of beach-bar deposits were developed in the southern gentle slope belt (Jiang et al., 2011), while a set of semi-deep to deep lacustrine mudstone and hydrocarbon source rocks were developed in the centre of the lake.

3. Methodology

Thirty-two red-bed sandstone samples and 39 Gy-bed sandstone samples were investigated from the Eocene Dongying Depression. Samples were impregnated with blue resin before thin sectioning in order to highlight pores. Carbonate minerals were distinguished in the thin sections through staining with Alizarin Red S and K-ferricyanide. Petrographic compositions and pores were determined using point counting method by counting 300 points per thin section.

Fifty-one red-bed mudstone and 12 Gy-bed mudstone samples were collected for mineralogical analyses using X-ray diffraction (XRD). A D8 DISCOVER from China University of Petroleum (East China) was used for XRD analysis with Cu-Ka radiation, a voltage of 40 kV, and a current of 25 mA. Prior to analysis each sample was oven-dried at 40 °C for 2 days and ground to<40 μm using an agate mortar to thoroughly disperse the minerals. In order to analyze the compositions of clay minerals, the samples were put in a plastic bottle, soaked in distilled water, and then disintegrated with an oscillator. Distilled water was added to the sample until the conductivity is less than 50 μs, and the suspension was separated by a centrifuge at a speed of 2000 r/min for 2 min. The granular suspension less than 2 μm was filtered with a ceramic filter, and then the clay mineral particles were placed in an oven to dry at 50 °C. No chemical pre-treatment was employed. Samples were scanned from 3° to 70° with a step size of 0.02°. Analysis of the XRD data provides relative abundances (in weight percent) of the various clay mineral phases. Eight samples were analyzed using a Hitachi S-4800 scanning electron microscope under the conditions of 20 °C, 35%RH, and 5.0 kV.

Based on thin section studies of the carbonate cement types and occurrence, samples with a high proportion of carbonate cement were selected to perform carbon and oxygen isotope analyses. Because the carbonate cements in this study were mainly composed of calcite, ferrocalcite, dolomite and ankerite, the particle size range was strictly controlled during the sample preparation to avoid interferences and cross contamination between the two mineral phases. The selected 31 red-bed and 18 Gy-bed samples were first ground below 200 mesh and then filtered through a 325 mesh sieve. After that the grains used for analysis were mostly approximately 5 μm–44 μm CO_2 was extracted using the stepwise reaction method of Al-Aasm et al. (1990). The carbon and oxygen isotopes of CO_2 were analyzed using a Finnigan Mat 252 mass spectrometer at the Chinese Academy of Geological Sciences. The Peedee belemnite (PDB) standard was used for the carbon isotope analysis, while the standard mean ocean water (SMOW) standard was used for the oxygen isotope analysis. The precisions of the carbon and oxygen isotope ratios were ±0.2‰ and ±0.3‰, respectively. The oxygen isotope ratios using the PDB standard were calculated using the equation $\delta^{18}O_{v\text{-}SMOW} = 1.03086 \times \delta^{18}O_{v\text{-}PDB} + 30.86$. The precisions of the carbon and oxygen isotope ratios were ±0.2‰ and ±0.3‰, respectively.

Fluid inclusion microthermometry was conducted using a Linkam Scientific THMSG-600 Geology System heating-freezing stage at China University of Petroleum (East China). Calibration of the stage was performed following the method outlined by MacDonald and Spooner (1981). In addition, synthetic fluid inclusion standards were used (pure CO_2 and water). The precision was ±0.2 °C at −56.5 °C and ±2 °C at 300 °C. The last ice melting temperatures (T_{mice}), and homogenization temperatures (T_h) were observed at a heating rate of up to 5 °C/min.

4. Results

4.1. Petrological compositions

The detrital compositions of the Es4x red-bed and Es4s gray-bed clastic reservoirs are summarized in Table 1. They are mainly lithic arkoses according to the Folk (1980) classification scheme, with corresponding average compositions being $Q_{42.5}F_{35.1}R_{23.7}$ and $Q_{45}F_{34.9}R_{20.1}$, respectively (Fig. 3A). There is no obvious difference of detrital components between the red-bed and gray-bed clastic reservoirs.

XRD compositions of the Eocene red-bed and gray-bed mudstones are shown in Table 2. There is little difference in the content of detrital components between the red-bed and gray-bed mudstones (Fig. 3B). Compared with gray-bed mudstone, the red-bed mudstone has a higher content of carbonates (especially ankerite) and sulfates (Fig. 3B and Table 2). Illite and chlorite in the red-bed mudstone are significantly higher than those in the gray-bed mudstone, whereas the illite-smectite mixed layer clays in the red-bed mudstone is lower than that in the gray-bed mudstone (Table 2).

4.2. Diagenetic characteristics and differences in sandstones

4.2.1. Dissolution

Dissolution in the red-bed and gray-bed sandstones mainly occurred in feldspar and quartz (Fig. 4A–F). The content of dissolution pores is summarized in Table 1. The total content of dissolution pores in the red-bed (0.04%–2.6%, av. 1.04%) and gray-bed (0.09%–2.65%, av. 1.03%) sandstones are similar, but the compositions of dissolution pores in the red-bed and gray-bed sandstones are different (Fig. 5). The content of feldspar dissolution pores in the red-bed sandstone is less than that in gray-bed sandstone. The content of quartz dissolution pores in the red-bed sandstone is more than that in gray-bed sandstone. Therefore, feldspar dissolution pores dominate the dissolution pores in the gray-bed

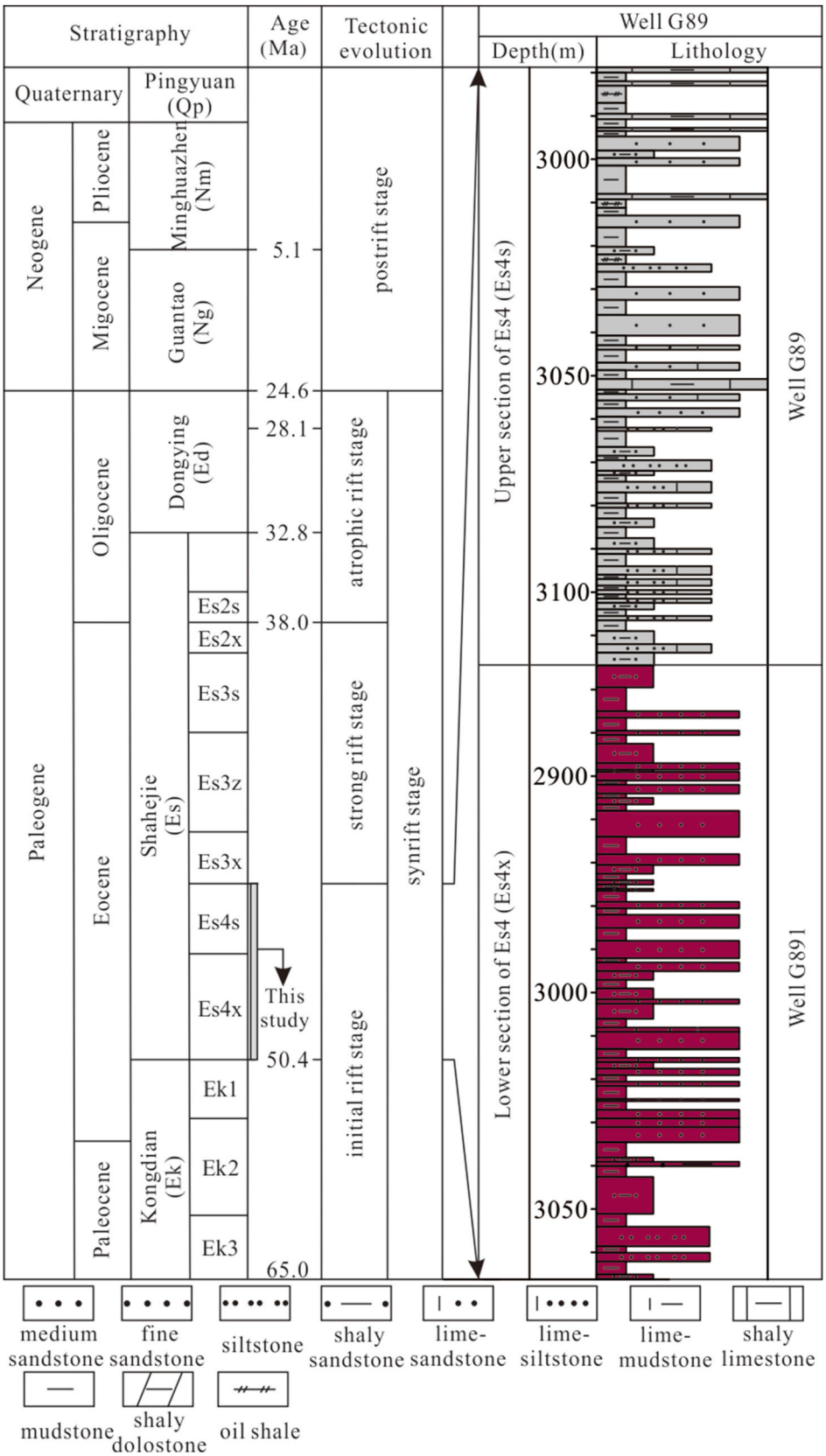

Fig. 2. Schematic Tertiary stratigraphy of the Dongying Depression in the Bohai Bay Basin. The Es4x unit comprises a red-bed sandstone and mudstone interval, while the Es4s unit comprises a gray-bed sandstone and mudstone interval. (For interpretation of the references to colour in this figure legend, the reader is referred to the Web version of this article.)

Table 1
Modal composition of the Eocene red-bed and gray-bed sandstones in the Dongying Depression.

	Red-bed sandstone			Gray-bed sandstone		
	Min	Max	Mean	Min	Max	Mean
Detrital grains						
Quartz (vol. %)	34	55.1	42.5	24.1	53.5	45
Potassium feldspars (vol. %)	10.1	22	16.7	8.4	25.6	16.8
Plagioclase feldspars (vol. %)	15.3	22.3	18.4	8.8	30.2	17.1
Volcanic lithic fragments (vol. %)	0.7	34.6	6.3	1.3	45.7	7.9
Metamorphic lithic fragments (vol. %)	5.2	30.4	12.2	5.1	19.6	10
Sedimentary lithic fragments (vol. %)	0	17.7	5.2	0	16.7	2.2
Mica (vol. %)	0.1	4.3	0.7	0	2.5	0.1
Diagenetic alterations						
Dissolution						
Feldspar dissolution pores (vol. %)	0.02	1.9	0.74	0.08	2.5	0.92
Quartz dissolution pores (vol. %)	0	0.75	0.18	0	0.35	0.11
Cementation						
Calcite (vol. %)	0.33	22.23	7.47	0.5	20.2	5.5
Ferrocalcite (vol. %)	0	6.4	1.8	0	5.7	2.05
Dolomite (vol. %)	0	7.67	0.55	0	17.4	2
Ankerite (vol. %)	0	3	0.21	0	2.3	0.95
Gypsum and Anhydrite (vol. %)	0	23	1.87	0	0	0
Quartz overgrowth (vol. %)	0	1.2	0.4	0	3.5	0.2
Clay minerals (wt. %)	2.4	14.1	3.4	0	15	2.7
Kaolinite (%)	7	56	19.27	1	38	23.3
Illite (%)	6.67	38.33	23.1	25	71	43
Illite-smectite mixed layers (%)	15.67	69.33	45.13	3	53	26.7
Chlorite (%)	5	28.33	12.5	1	20	7
Pyrite (vol. %)	0	4.67	0.8	0	5.6	0.25

sandstone, while quartz dissolution pores play an important role in dissolution pores in the red-bed sandstone (Fig. 5).

4.2.2. Cementation

The types of cements in the red-bed and gray-bed sandstones are mainly carbonates (including calcite, ferrocalcite, dolomite and ankerite), authigenic quartz, gypsum and anhydrite, and clay minerals (Fig. 4D-O). The contents of cements are summarized in Table 1.

Carbonate cements are the majority type in both the red-bed and gray-bed sandstones with extremely heterogeneous distributions. The content of ferro-calcite, dolomite and ankerite is lower in the red-bed sandstone than that in the gray-bed sandstone. The content of carbonate cements decreases rapidly from the sandstone-mudstone contact to the centre of sandstone beds (Fig. 6A and B), while the percentage of ferro-carbonate in the total carbonate cement increases gradually from the sandstone-mudstone contact to the centre of sandstone beds (Fig. 6C). Tight carbonate cemented layers composed of coarse-crystalline calcite (Fig. 4G and H) are developed in sandstones along the sandstone-mudstone contact. The tightly cemented layer in red-bed sandstone is thicker than that in gray-bed sandstone (Fig. 6A and B). There is nearly no ferro-carbonate cement at the boundary of red-bed sandstone or within 0.3 m to the contact (Fig. 6C). Whether at the boundary or the centre of the sandstone, the percentage of ferro-carbonate in the total carbonate cement in the gray-bed sandstone is more than that in the red-bed sandstone (Fig. 6C).

The carbon and oxygen isotopic compositions of carbonate cements in the red-bed and gray-bed sandstones are shown in Fig. 7. The $\delta^{13}C$ of calcite-ferrocalcite and dolomite-ankerite in the red-bed and gray-bed sandstone is −0.5‰~-16.3‰ (av. −7.3‰), −6.6‰~-20.7‰ (av. −11.8‰), −2.5‰~-13.6‰ (av. −6.3‰) and 0.3‰~-10.3‰ (av. −3.8‰), respectively. The $\delta^{18}O$ of calcite-ferrocalcite and dolomite-ankerite in the red-bed and gray-bed sandstone is −6.8‰~-15.2‰ (av. −11.3‰), −9.3‰~-13.6‰ (av. −12.2‰), −10.4‰~-14.7‰ (av. −12.6‰) and −7.6‰~-13.1‰ (av. −10.4‰), respectively. From the contact to the centre of sandstone beds, both the $\delta^{13}C$ and $\delta^{18}O$ of calcite-ferrocalcite and dolomite-ankerite become lighter (Fig. 7A and B), which has a good correspondence with the percentage of ferro-carbonate in the sandstones (Fig. 7C). The $\delta^{18}O$ of calcite and ferro-calcite at the boundary of red-bed sandstone is heavier than that at the boundary of the gray-bed sandstone (Fig. 7A and B).

Table 2
The compositions of the Eocene red-bed and gray-bed mudstones in the Dongying Depression.

	Red-bed mudstone			Gray-bed mudstone		
	Min	Max	Mean	Min	Max	Mean
Quartz (wt. %)	20	41	28.4	20	33	27.8
Potassium feldspars (wt. %)	1	24	6.1	0	15	5.0
Plagioclase feldspars (wt. %)	5	9	5.8	8	21	14.0
Calcite (wt. %)	0	18	11.6	7	16	12.1
Dolomite (wt. %)	0	4	1.4	0	4	1.9
Ankerite (wt. %)	0	50	7.7	0	20	4.1
Clay (wt. %)	12	48	34.5	11	53	34.1
Kaolinite (%)	0	11.8	4.2	0	9	3.8
Illite-smectite mixed layer clays (%)	9.5	40.5	24.3	33	80	55.7
Illite (%)	18.3	70.7	51	16	65	33.3
Chlorite (%)	13	53.3	20.5	2	16	5.3
Pyrite (wt. %)	0	5	0.6	0	3	1.1
Gypsum/anhydrite (wt. %)	0	15	1.5	–	–	–
Halite (wt. %)	0	2	0.7	–	–	–
Hematite (wt. %)	0	4	1.7	–	–	–

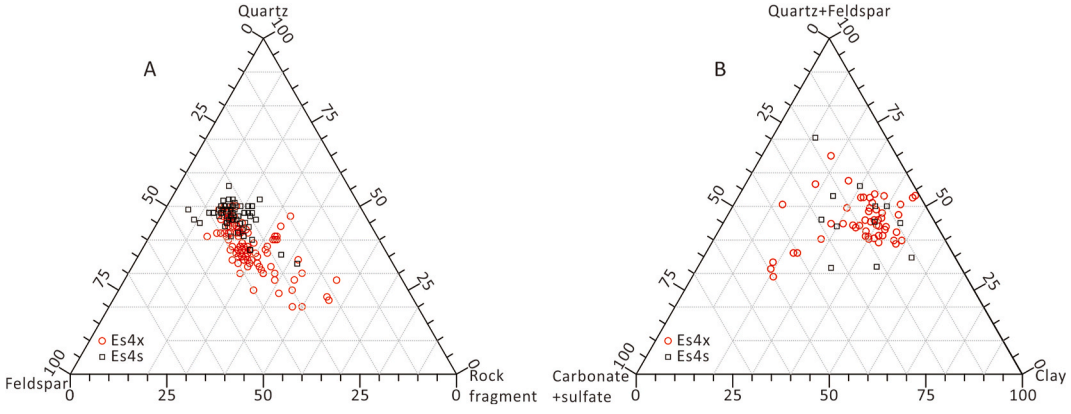

Fig. 3. Rock and mineral composition triangular diagram of the Eocene red-bed and gray-bed sandstones (A) and mudstones (B) in the Dongying Depression. (For interpretation of the references to colour in this figure legend, the reader is referred to the Web version of this article.)

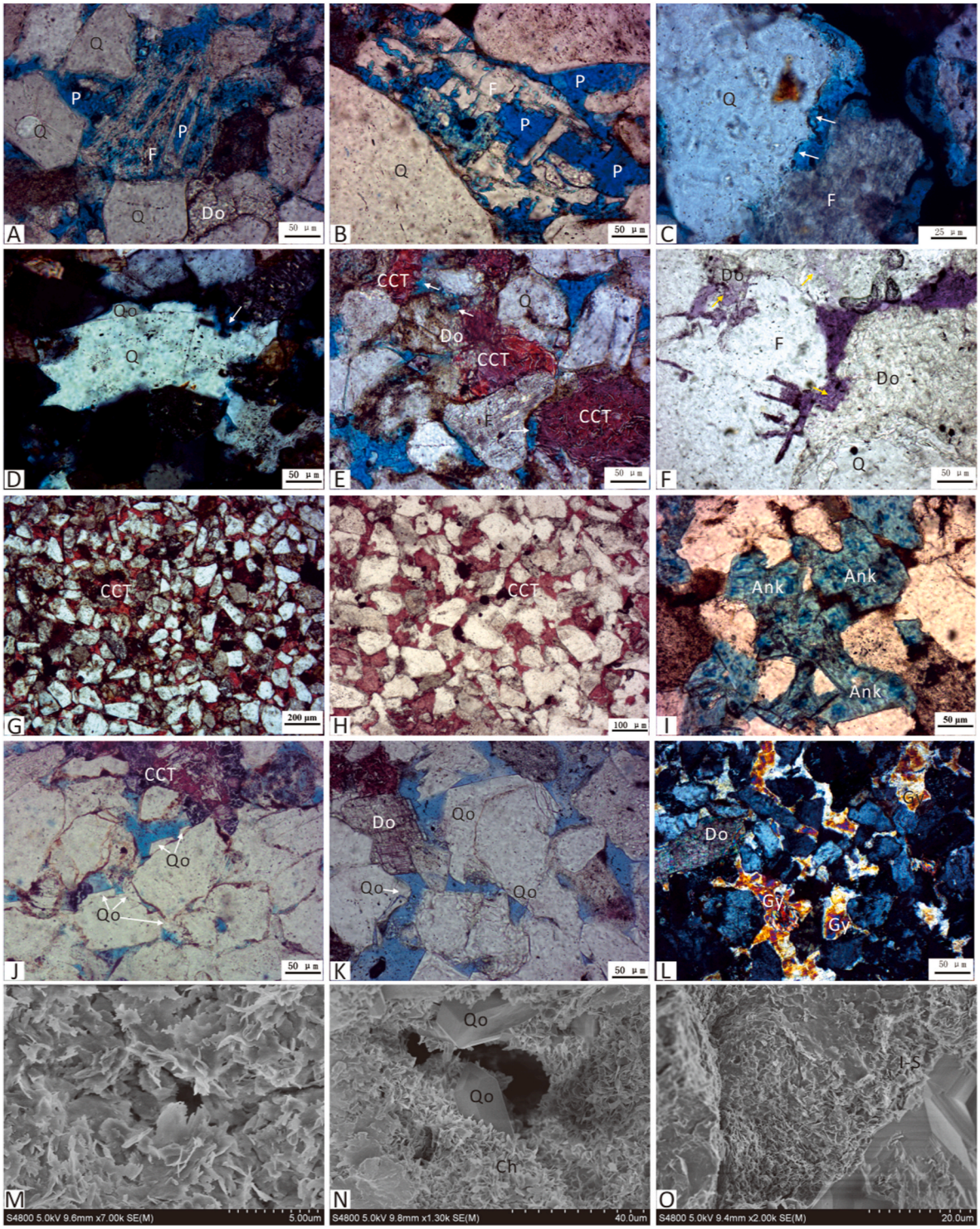

Fig. 4. Photos from thin sections show types of diagenesis in the Eocene red-bed and gray-bed reservoirs in the Dongying Depression. (A) Feldspar dissolution pores (−) from well Guan113 at 2483.53 m, Es4x; (B) Feldspar dissolution pores (−) from well B168 at 2386.3 m, Es4s; (C) Quartz dissolution pores (arrows) (+) from well WX131 at 2368 m, Es4x; (D) Quartz dissolution pores of (arrow) (−) from well F119 at 3292.55 m, Es4s; (E) Dissolution pores of calcite (arrows) (−) from well W130 at 2081.4 m, Es4x; (F) Dissolution pores of calcite (arrows) (−) from well W125 at 2386.3 m, Es4s. (G) Coarse-crystalline calcites filling intergranular pores (−) from well Wx99 at 2093.04 m, Es4x; (H) Coarse-crystalline calcites filling intergranular pores (−) from well G351 at 2455.14 m, Es4s; (I) Ankerites filiing intergranular pores (−) from well F154 at 3513 m, Es4s; (J) Quartz overgrowth and calcite cements (−) from well Guan120 at 2945.79 m, Es4x; (K) Quartz overgrowth and dolomite cements (−) from well G890 at 2599.2 m, Es4s; (L) Gypsum and anhydrite and dolomite cements (+) from well Guan120 at 2950.09 m, Es4x; (M) Illite-smectite mixed layer clays from well Guan113 at 2483.53 m, Es4x; (N) Chlorite and quartz overgrowth from well Guan120 at 2945.79 m, Es4x; (O) Illite-smectite mixed layer clays from well G890 at 2599.2 m, Es4s. Q-quartz, F-feldspar, CCT-calcite, Do-dolomite, Qo-quartz overgrowth, Gy-gypsum and anhydrite, Ch-chlorite, I–S- illite-smectite mixed layers, P-pores, (−)-polarized light, (+)-crossed polarizers. See Fig. 1B for well locations. (For interpretation of the references to colour in this figure legend, the reader is referred to the Web version of this article.)

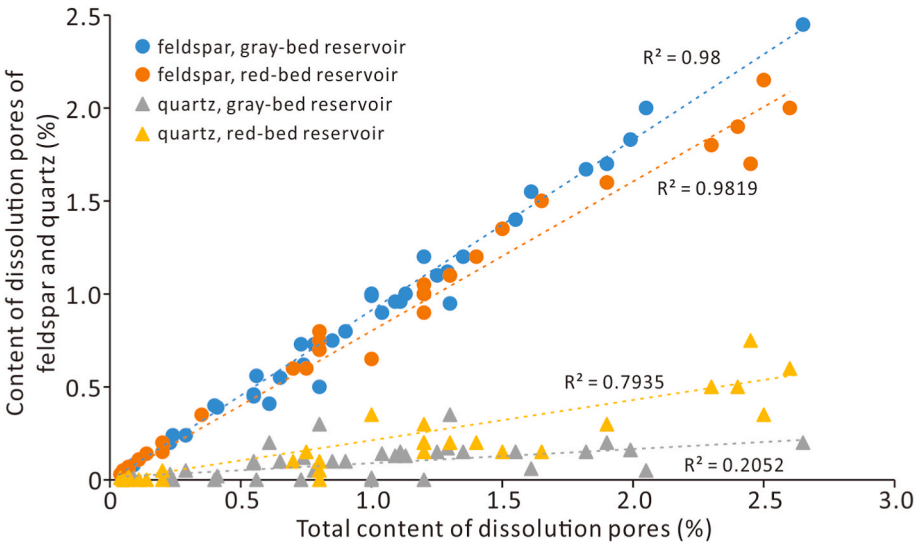

Fig. 5. Correlations between total content of dissolution pores and content of dissolution pores of feldspar, carbonate and quartz in the red-bed and gray-bed sandstones. (For interpretation of the references to colour in this figure legend, the reader is referred to the Web version of this article.)

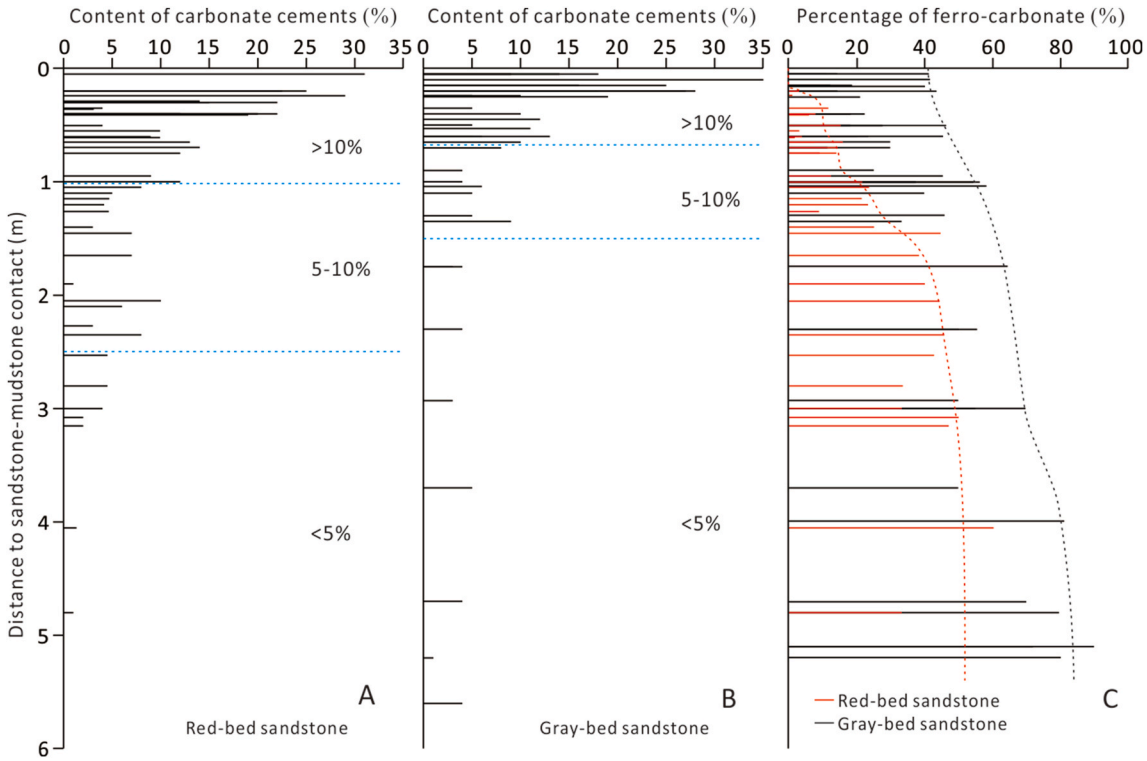

Fig. 6. Content of carbonate cements and percentage of ferro-carbonate in the total carbonate cement from the sandstone-mudstone contact to the centre of the red-bed and gray-bed sandstone. (For interpretation of the references to colour in this figure legend, the reader is referred to the Web version of this article.)

Authigenic quartz in the red-bed and gray-bed sandstones mainly occurs as quartz overgrowth with low contents (Fig. 4D, J, K, N). However, the content of quartz overgrowths in the red-bed sandstone is higher than that in the gray-bed sandstone (Table 1). The fluid inclusion microthermometry shows that the homogenization temperatures (T_h) of liquid-rich two-phase aqueous inclusions in quartz overgrowths in the red-bed and gray-bed sandstones are mainly in the range of 90–130 °C (Fig. 8). The average T_h (112.5 °C) of inclusions in quartz overgrowths in the red-bed sandstone is slightly higher than that in the gray-bed sandstone (108.3 °C).

Gypsum and anhydrite are unique cements in the red-bed sandstones occurring as coarse-grain fillings in intergranular pores (Fig. 4L). The content of gypsum and anhydrite also decreases away from the sandstone-mudstone contact (Fig. 9). The sulfur isotopic composition ($\delta^{34}S_{CDT}$ (‰)) of gypsum and anhydrite in the red-bed sandstone is in the range of 21.2‰–37.8‰ (av. 33.5‰) (Ma et al., 2016).

Illite contents in the gray-bed sandstone are more than those in the red-bed sandstones, while illite-smectite mixed layer clay and chlorite in the red-bed sandstones are more than those in the gray-bed sandstones (Table 1).

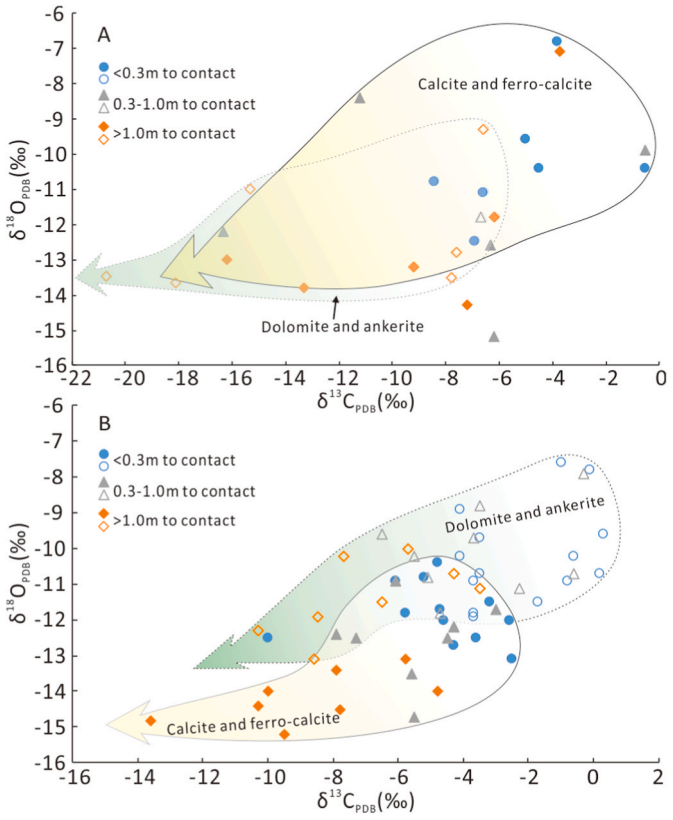

Fig. 7. Correlations of carbon and oxygen isotopic compositions of carbonate cements in the Eocene red-bed and gray-bed sandstone in the Dongying Depression. (For interpretation of the references to colour in this figure legend, the reader is referred to the Web version of this article.)

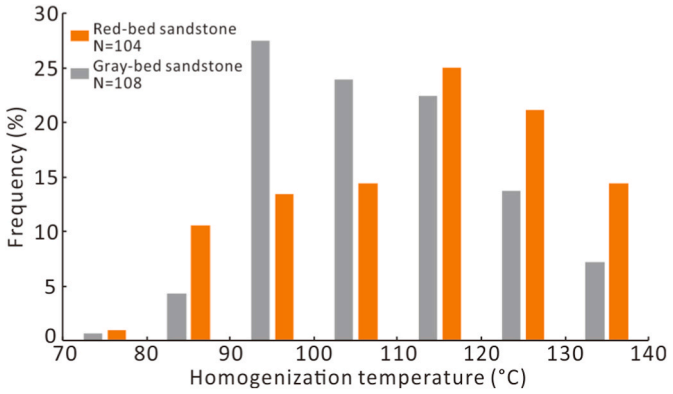

Fig. 8. Frequency distribution histograms showing homogenization temperatures for liquid-rich two-phase aqueous inclusions in quartz overgrowths in the Eocene red-bed and gray-bed sandstones in the Dongying Depression. (For interpretation of the references to colour in this figure legend, the reader is referred to the Web version of this article.)

4.3. Vertical distribution of clay minerals in mudstone

The vertical changes of kaolinite and chlorite in the red-bed mudstone are not obvious (Fig. 10). The content of kaolinite in the red-bed mudstones is usually less than 20%, chlorite content is usually more than 35%, illite content is less than 20% but increased to 40% below the depth of 2250 m, and the ratio of I–S is more than 40% but sharply deceased to 20% below the depth of 2250 m (Fig. 10). The clay minerals were dominated by kaolinite and I–S mixed layers in the gray-bed sandstones above the depth of 2650 m. The content of chlorite and illite increased and the kaolinite and ratio of I–S decreased obviously below the depth of 2650 m (Fig. 10).

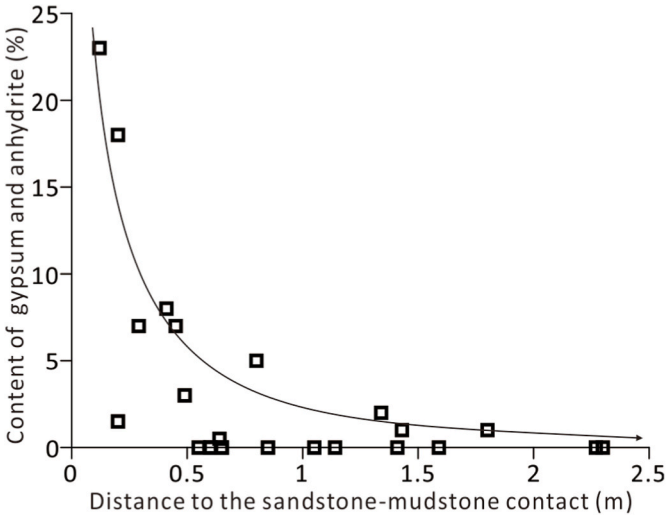

Fig. 9. Distribution of gypsum and anhydrite from the sandstone-mudstone contact to the centre of the red-bed sandstone.

4.4. Reservoir properties

Point counting of thin sections indicate that the reservoir space in the red-bed sandstone is dominated by primary pores (Fig. 11A). The percentage of dissolution pores in the total reservoir pores in the red-bed sandstone is usually less than 50% (Fig. 11B). The content of primary pores in the gray-bed sandstones decreases gradually with increasing burial depth, while the content of dissolution pores increases gradually with increasing burial depth (Fig. 11). Above 2500 m, the reservoir space is dominated by primary pores in gray-bed sandstone, while below 2500 m, dissolution pores are dominant (Fig. 11).

5. Discussion

Diagenesis in clastic reservoirs is controlled by various factors, among which petrological composition, burial pattern, temperature, formation pressure and diagenetic fluid properties play important roles (Wilkinson et al., 1997; Osborne and Swarbrick, 1999; Rossi et al., 2002; Karim et al., 2010; Wang et al., 2016, 2018; Caracciolo, 2020). There is no obvious difference in petrological composition, burial pattern and the formation pressure between the red-bed and gray-bed sandstones in the Dongying Depression (Fig. 3A; Wang et al., 2016, 2017). Although the paleogeothermal gradient of the red beds is slightly higher than that of the gray beds (Qiu et al., 2004), the temperature mainly affects diagenesis through influencing water-rock interactions (Karim et al., 2010). All of these suggest that diagenetic fluid properties controlled the diagenetic differences and diagenetic evolution of the red-bed and gray-bed sandstone reservoirs during the burial process. The evolution of diagenetic fluid in clastic reservoirs during the burial process usually starts from connate water, which was controlled by the sedimentary environment.

5.1. Influence on eodiagenesis

The precipitation temperatures of the calcite cements in the red-bed and gray-bed sandstones were calculated using the $\delta^{18}O_{VPDB}$ values of the calcite cements (Friedman and O'Neil, 1977) and assuming that the $\delta^{18}O_{V\text{-}SMOW}$ values for the pore water is −2‰ to 0‰ (Wang et al., 2016, 2017). The precipitation temperatures of calcite cements within 0.3 m and 0.3–1 m from the sandstone-mudstone contact in the red-bed

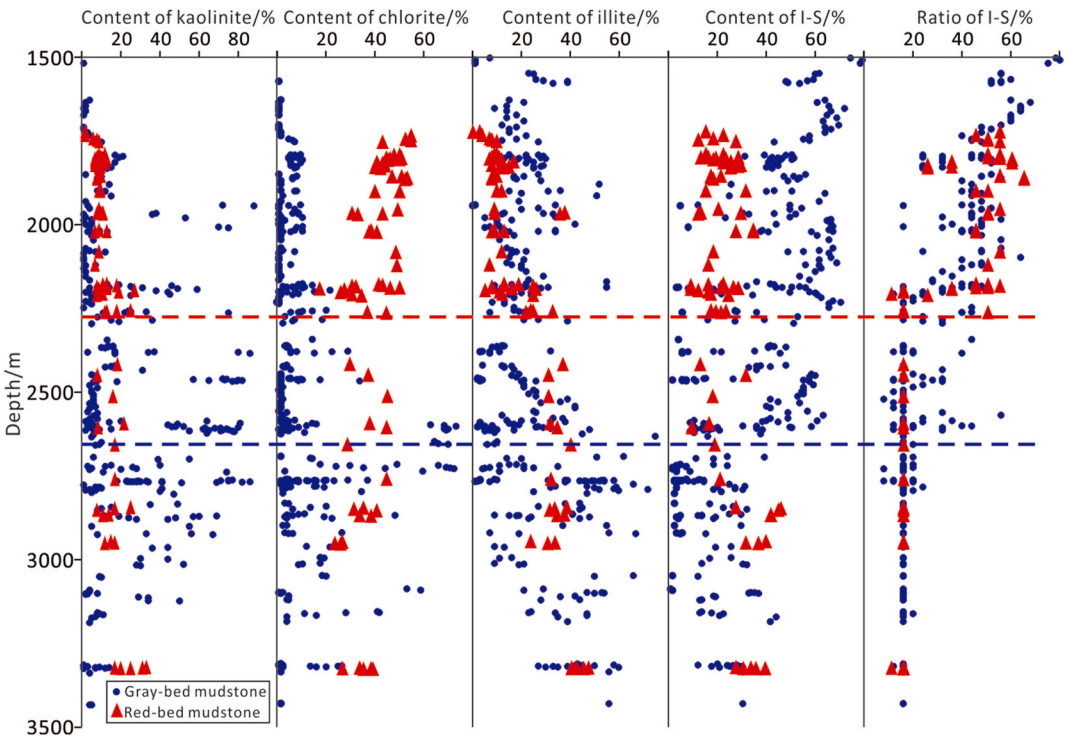

Fig. 10. Distribution of clay minerals in the Eocene red-bed and gray-bed mudstones in the Dongying Depression. (For interpretation of the references to colour in this figure legend, the reader is referred to the Web version of this article.)

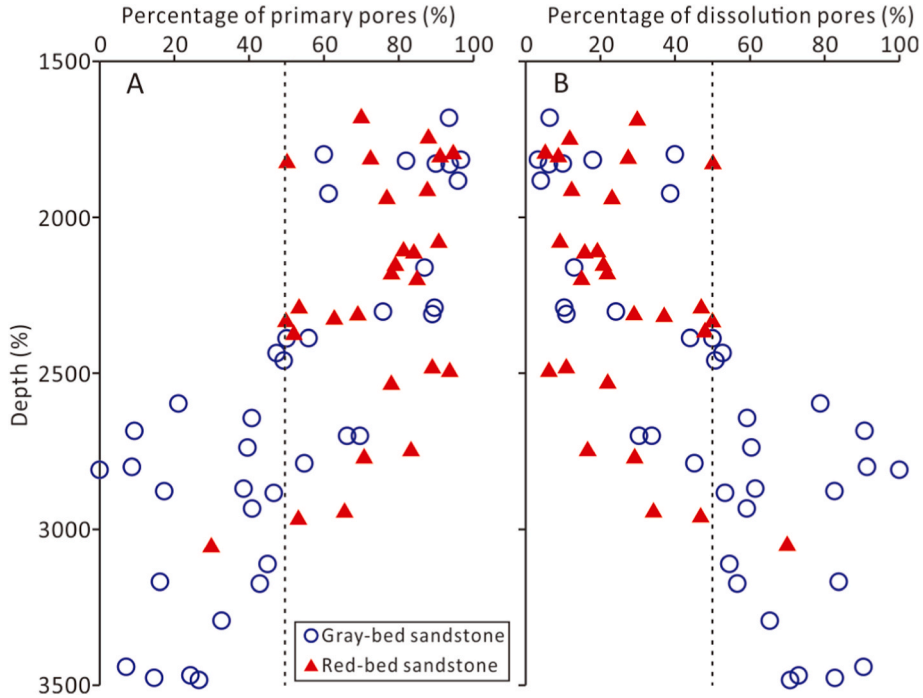

Fig. 11. Percentage of dissolution pores in the Eocene red-bed and gray-bed sandstone reservoirs in the Dongying Depression. (For interpretation of the references to colour in this figure legend, the reader is referred to the Web version of this article.)

sandstone are in the ranges of 39.8°C–85.2 °C (av. 66.6 °C) and 41.5°C–94.8 °C (av. 68.4 °C), respectively (Fig. 12A), and the clastic particles in strong calcite cemented sandstones are floating or show point contacts (Fig. 4G), which indicate that the calcite cements within 1 m from the sandstone-mudstone contact were precipitated during eodiagenesis. The precipitation temperatures of calcite cements within 0.3 m and 0.3–1 m from the sandstone-mudstone contact in the gray-bed sandstone are in the ranges of 62°C–99.4 °C (av. 80.8 °C) and 64.8°C–115.6 °C (av. 84.8 °C), respectively (Fig. 12C), which indicate that calcite cements within 1 m from the sandstone-mudstone contact were not completely precipitated during eodiagenesis. Therefore, compared with the gray-bed sandstone, eodiagenetic calcite

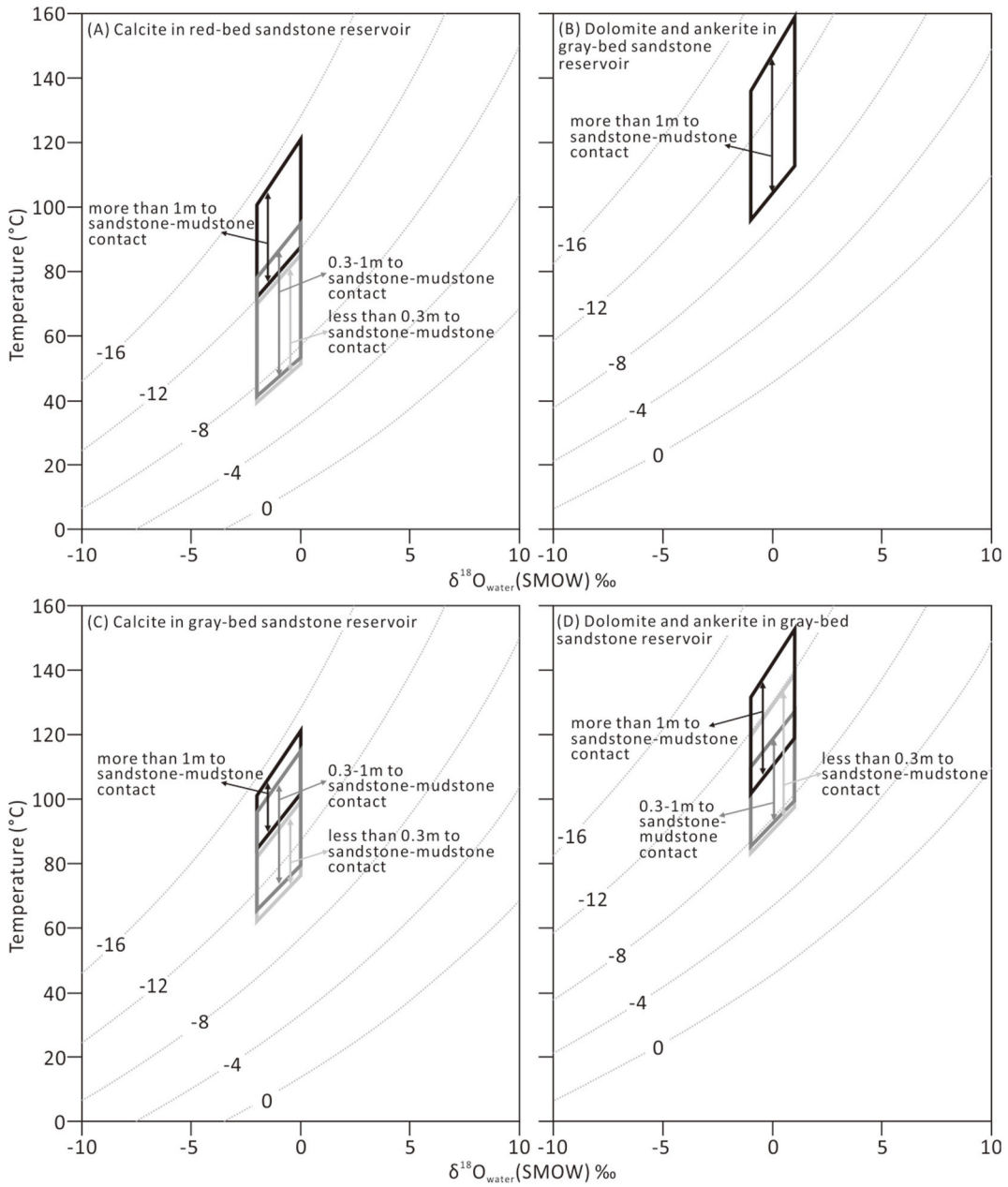

Fig. 12. Diagrams showing the range of temperatures calculated from the assumed oxygen isotopic composition of the pore water and $\delta^{18}O$ values of: (A) Calcite in the red-bed sandstone reservoir using the fractionation equation of Friedman and O'Neil (1977), (B) Dolomite and ankerite in the red-bed sandstone reservoir using the fractionation equation of Land (1983), (C) Calcite in the gray-bed sandstone reservoir using the fractionation equation of Friedman and O'Neil (1977), and (D) Dolomite and ankerite in the gray-bed sandstone reservoir using the fractionation equation of Land (1983).

cementation at the boundary of the red-bed sandstone is stronger.

The decreasing content of carbonate and sulfate cements from the sandstone-mudstone contact to the centre of sandstone beds (Fig. 6A and B and Fig. 9) indicates that the materials for the precipitation of calcite and gypsum at the boundary of sandstones were mainly from the adjacent mudstones during the shallow burial stage (Wang et al., 2016, 2018, 2019a, b). Connate water was the dominant controlling factor in the early stage diagenetic environment (Alagarsamy et al., 2005; Carvalho et al., 2014; Zhang et al., 2014). During the depositional period of Es4x, the clastic and evaporite deposits developed together; the salinity of the Dongying Depression was more than 40 g/L with abundant metal cations (e.g. Ca^{2+}, K^{+}, Na^{+}, Mg^{2+}) and the pH was more than 8.7 because of the arid and semiarid climate and evaporation environment (Wang et al., 2016, 2018). High water salinity and metal cation content and an alkaline environment are favorable for the transformation of clay minerals (Deconinck et al., 2014; Mefteh et al., 2014; Wang et al., 2016). The vertical distribution of clay minerals in the red-bed mudstones indicates that the transformation of clay minerals mainly occurred between the smectite and illite. The transformation between kaolinite and chlorite was not apparent (Fig. 10). During the transformation of smectite to illite, abundant metal cations such as Ca^{2+}, Na^{+}, Fe^{2+}, Mg^{2+} were released, which further increased the fluid salinity (Bristow and Milliken, 2011; Wang et al., 2016). The salinity of connate water decreased to 11.2 g/L during the depositional period of Es4s due to the relatively wet climate (Wang et al., 2017). Low water salinity makes the transformation of clay minerals in the gray-bed mudstone lag. During the diagenetic alteration of the interbedded mudstone, a lot of connate water and clay mineral transformation fluid were discharged to the adjacent sandstone, which caused calcite and gypsum cementation at the boundary of the sandstone (Zhang et al., 2014; Wang et al., 2016,

2018, 2019a, b). Due to the early higher salinity diagenetic fluids, the formation time of the tight carbonate cemented zone and the content of calcite at the boundary of the red-bed sandstone occurred earlier and were higher than those in the gray-bed sandstone (Fig. 6 A, B and Fig. 13).

The $\delta^{34}S_{CDT}$ of sulfate cements (gypsum and anhydrite) in the red-bed sandstone is heavier than that of contemporaneous marine evaporites (17.7‰–22.5‰) (Paytan et al., 2011), indicating that their precipitation corresponds to an evaporation environment (Paytan et al., 2011; Ma et al., 2016). The materials for the precipitation of sulfate cements were mainly from connate water within the mudstone. The dry climate and closed, strong evaporation lake water environment of the red beds may be the reason for the heavier sulfur isotope in the gypsum and anhydrite (Fig. 13).

When the strongly alkaline connate water was discharged from mudstone to sandstone, a large amount of quartz dissolution occurred in the adjacent red-bed sandstones (Fig. 5), which is the reason why the content of quartz dissolution pores in the red-bed sandstones is obviously higher than that in the gray-bed sandstones.

5.2. Influence on mesodiagenesis

The precipitation of dolomite and ankerite cements in the red-bed and gray-bed sandstones were calculated using the fractionation equation of Land (1983) and assuming that the $\delta^{18}O_{V\text{-}SMOW}$ values are −1‰ to 1‰ for the pore water (Wang et al., 2016, 2017). There is nearly no dolomite or ankerite in the red-bed sandstones within 1 m from the sandstone-mudstone contact. The precipitation temperatures of dolomite and ankerite in the gray-bed sandstones within the ranges of less than 0.3 m and 0.3m–1.0 m from the sandstone-mudstone contact are 83.3°C–138.8 °C (av. 112.6 °C) and 85.4°C–137.7 °C (av. 111.5 °C), respectively (Fig. 12B, D), which indicate that these cements were formed during the mesodiagenetic stage. The precipitation temperatures of calcite cements within 1 m from the sandstone-mudstone contact in the gray-bed sandstones also suggest that some of the calcite was precipitated during the mesodiagenetic stage (Fig. 12C). With the increasing burial depth and increasing formation temperature, clay mineral transformation in the gray-bed mudstone discharged abundant fluid with Ca^{2+}, Na^{+}, Fe^{2+}, Mg^{2+} that continued to enter the boundary of the gray-bed sandstone (Fig. 10; Bristow and Milliken, 2011; Wang et al., 2019a, b), and caused the precipitation of ferro-calcite, dolomite

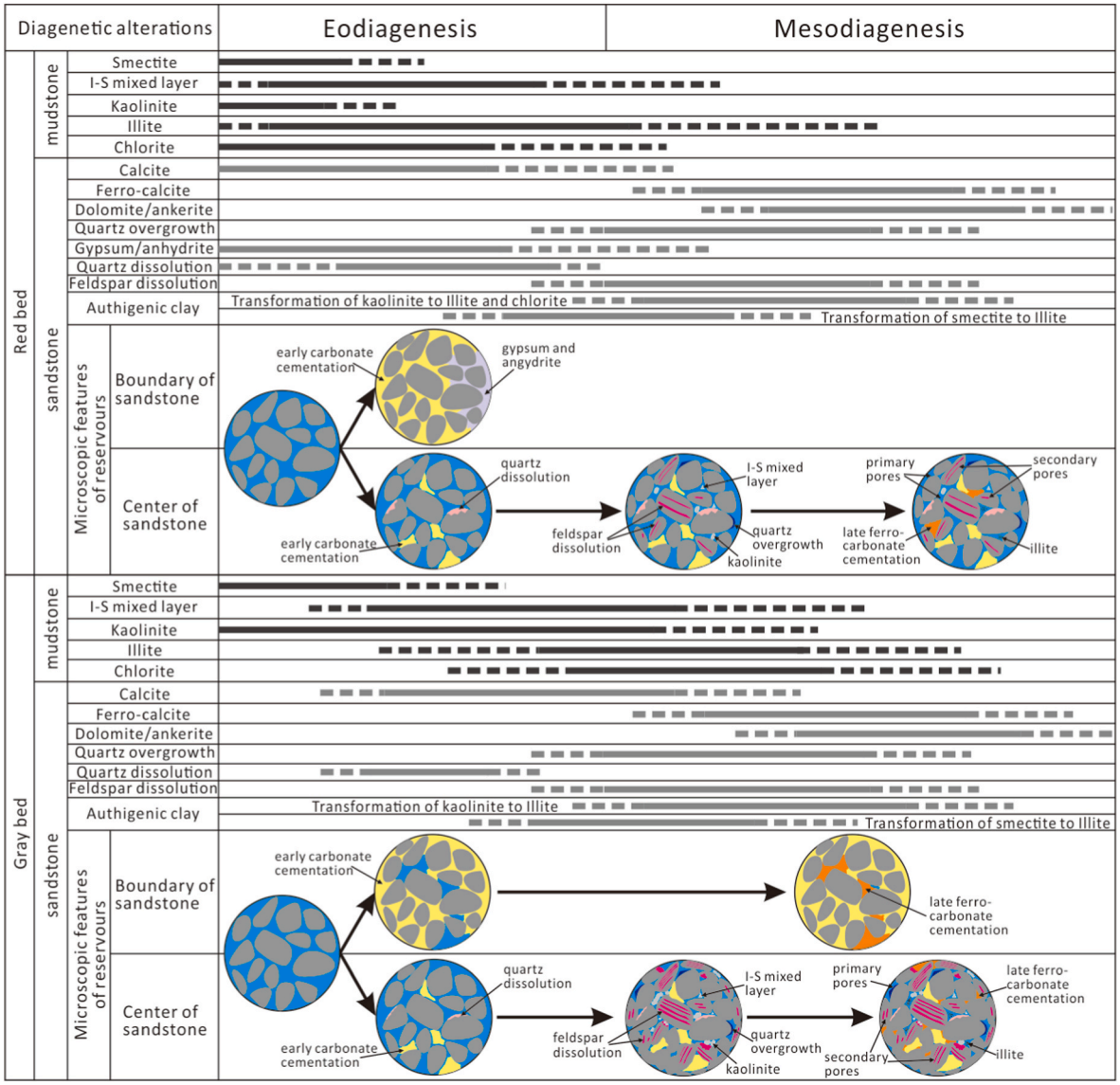

Fig. 13. Diagenetic alterations during the eodiagenetic and mesodiagenetic stages in the Eocene red-bed and gray-bed sandstone reservoirs. (For interpretation of the references to colour in this figure legend, the reader is referred to the Web version of this article.)

and ankerite. Although a small amount of fluid may have been produced in the red-bed mudstone during the mesodiagenetic stage, the early formation of tight carbonate cement zone at the boundary of the red-bed sandstones made it difficult for the later fluid to enter the boundary of the red-bed sandstone, which explains why the carbonate cement at the boundary of the red-bed sandstone only developed calcite (Figs. 7C and 13).

When the temperature was in the range of 80°C–120 °C, a large amount of organic acid and CO_2 generated by Es4s hydrocarbon source rocks (Morad et al., 2000; Heydari and Wade, 2002) was discharged into the red-bed and gray-bed sandstones through hydrocarbon source faults (Meng et al., 2011). Because of the tight carbonate cemented zone formed at the boundary of the sandstones, the organic acid and CO_2 were mainly concentrated in the central part of the sandstones. Fluid inclusion homogenization temperatures in quartz overgrowths are consistent with the favorable preservation temperatures of organic acid in both the red-bed and gray-bed sandstones (Fig. 8), indicating that the red-bed and gray-bed sandstones were affected by the organic acid at the same time (Fig. 13). After the organic acid enters the reservoir, it first neutralizes the early strong alkaline pore fluid in the red-bed sandstones, and then causes feldspar dissolution and authigenic quartz cementation in the central part of the sandstones (Wang et al., 2016, 2018). That's why the content of feldspar dissolution pores in the red-bed sandstone was lower than that in the gray-bed sandstone (Figs. 5 and 13).

The precipitation temperatures of calcite and ferro-calcite more than 1 m in towards the centre of the red-bed and gray-bed sandstones are 72°C–121 °C (av. 95.2 °C) and 84.7°C–121 °C (100.8 °C), respectively, whereas the precipitation temperatures of dolomite and ankerite in the same part of the sandstones are 96.1°C–159 °C (av. 132.7 °C) and 101.7°C–152.7 °C (122.7 °C), respectively, suggesting that these carbonate cements were precipitated during the mesodiagenetic stage (Fig. 12). The light carbon isotope compositions indicate that the precipitation of carbonate cements in the central part of the red-bed and gray-bed sandstones was affected by organic CO_2 (Fig. 7). Ca^{2+} produced by feldspar dissolution and Fe^{2+}, Mg^{2+} carried by organic acid and transformed from clay minerals can provide source material for the formation of carbonate cement in the central part of the sandstones (Wang et al., 2019a, b). When the formation temperature was more than 120 °C, the decarboxylation of organic acids gradually took place to make the fluid become alkaline again (Heydari and Wade, 2002), which caused the precipitation of the late carbonate cement. Due to the higher amount of feldspar dissolution, the content of carbonate cements and percentage of ferro-carbonate in the gray-bed sandstone was higher than that in the red-bed sandstone (Figs. 6 and 13).

5.3. Influence on diagenetic sequence and reservoir properties

As mentioned above, the sedimentary environment not only directly affected the eodiagenesis, but also affected the mesodiagenesis through the differences caused by eodiagenesis. Under the influence of high salinity and strong alkaline connate water in an arid climate, the boundary of red-bed sandstone was cemented tightly by calcite and gypsum/anhydrite during the eodiagenetic stage, and the reservoir porosity decreased rapidly to less than 5%. In the mesodiagenetic stage, it was difficult for formation-fluid to enter the tightly cemented zone, resulting in a single episode of diagenesis at the boundary of the red-bed sandstone (Fig. 13). A small amount of eodiagenetic calcite was precipitated in the centre of the red-bed sandstone. Influenced by the strong alkaline connate water, many quartz dissolution pores developed in the centre of the red-bed sandstone during the eodiagenetic stage (Fig. 13). Affected by the early tight calcite cemented zone at the boundary of the red-bed sandstones, the later diagenetic fluids were confined in the centre of the thick red-bed sandstones. Therefore, the centre of the red-bed sandstone experienced a diagenetic sequence of weak eodiagenetic calcite cementation/strong eodiagenetic quartz dissolution, weak mesodiagenetic feldspar dissolution/authigenic quartz and kaolinite cementation, weak mesodiagenetic ferro-carbonate and illite cementation (Fig. 13). Tight calcite cemented zones formed during the eodiagenetic stage could resist compaction to a large extent, and thus preserved a large number of intergranular pores in the centre of the sandstones during the mesodiagenetic stage. In addition, the content of dissolution pores is low, so the reservoir space of the red-bed sandstone mainly consists of primary pores (Fig. 11).

During the depositional period of the gray beds, the paleoclimate was relatively humid and the salinity of connate water was obviously reduced. Although the eodiagenetic calcite cementation was developed at the boundary of the gray-bed sandstone, the degree was weak, and a certain number of intergranular pores were still left (Fig. 13). A small amount of eodiagenetic calcite was also precipitated in the centre of the gray-bed sandstone. Clay minerals in the gray-bed mudstone were further transformed during the mesodiagenesis, a large number of metal ions entered the reservoir, filling the residual intergranular pores at the boundary of the gray-bed sandstone with ferro-carbonate cements, which further reduced the porosity of the reservoir and made the boundary of the gray-bed sandstone tightly cemented (Fig. 13). The strong dissolution of feldspar provided a large amount of Ca^{2+}, which caused more ferro-carbonate cements to be precipitated in the central part of the gray-bed sandstone. Therefore, the boundary of the gray-bed sandstone experienced a diagenetic sequence of eodiagenetic calcite cementation, and mesodiagenetic ferro-carbonate cementation (Fig. 13). The centre of the gray-bed sandstone experienced a diagenetic sequence of weak eodiagenetic calcite cementation and quartz dissolution, strong mesodiagenetic feldspar dissolution/authigenic quartz and kaolinite cementation, relatively strong mesodiagenetic ferro-carbonate and illite cementation (Fig. 13). Due to the later formation time and thin carbonate cemented zone at the boundary of the gray-bed sandstone, a large number of intergranular pores were destroyed by compaction in the centre of the sandstone during the burial process. Because of the high content of dissolution pores the reservoir space in the gray-bed sandstone is dominated by secondary pores below the depth of 2500 m (Fig. 11).

6. Conclusions

By comparing the diagenetic differences between the red-bed sandstones deposited in an arid environment and the gray-bed sandstones deposited in a relative humid environment, it is shown that the sedimentary environment had an obvious influence on the reservoir diagenetic evolution and reservoir properties. Sedimentary environment affects reservoir diagenetic evolution through influencing the chemical properties of connate water, the transformation rate and degree of clay minerals in interbedded mudstone, and the properties of the diagenetic fluid during burial process.

The Eocene red-bed sandstone reservoirs were characterized by strong eodiagenetic calcite and gypsum/anhydrite cementation at the boundary of sandstone and relatively strong quartz dissolution and weak mesodiagenetic feldspar dissolution and ferro-carbonate cementation in the centre of the sandstone. The reservoir spaces of the red-bed sandstones were dominated by primary pores. Eodiagenetic calcite cementation at the boundary of the gray-bed sandstone and quartz dissolution were relatively weak and the carbonate cemented zone at the boundary of the gray-bed sandstone was strengthened by mesodiagenetic ferro-carbonates. Relatively strong feldspar dissolution and ferro-carbonate cementation occurred in the centre of the gray-bed sandstones. The reservoir spaces of the gray-bed sandstones below the depth 2500 m were dominated by secondary pores.

Credit author statement

Jian Wang: Conceptualization, Methodology, Writing – original draft, Writing – review & editing. **Yuhan Pang**: Data curation, Visualization. **Yingchang Cao**: Supervision. **Jie Peng**: Data curation,

Investigation. **Keyu Liu**: Writing – review & editing. **Huimin Liu**: Resources.

Declaration of competing interest

The authors declare that they have no known competing financial interests or personal relationships that could have appeared to influence the work reported in this paper.

Acknowledgement

This work was co-funded by the National Key Research and Development Program of China (Grant No. 2019YFC0605501), Natural Science Foundation of China (Grant No. 418210002), the Shandong Provincial Natural Science Foundation (ZR2019MD004), the Fundamental Research Funds for the Central Universities and the Development Fund of Key Laboratory of Deep Oil & Gas (20CX02102A), and the Strategic Priority Research Program of the Chinese Academy of Sciences (Grant No. XDA14010301). We are also grateful to the Geosciences Institute of the Shengli Oilfield, SINOPEC, for permission to access their in-house database, providing background geologic data and permission to publish the results.

Appendix A. Supplementary data

Supplementary data to this article can be found online at https://doi.org/10.1016/j.marpetgeo.2021.105153.

References

Al Gahtani, F., 2013. The influence of diagenetic alterations on porosity in the Triassic Narrabeen group, southern Sydney basin, Australia. Geol. Q. 57, 613–628.
Al-Aasm, I.S., Taylor, B.E., South, B., 1990. Stable isotope analysis of multiple carbonate samples using selective acid extraction. Chem. Geol. 80, 119–125.
Alagarsamy, R., Wolff, G.A., Chester, R., 2005. Partitioning and speciation of trade metal diagenesis in differing depositional environments in the sediments of the Oman Margin. Aquat. Geochem. 11 (2), 195–213.
Bristow, T.F., Milliken, R.E., 2011. Terrestrial perspective on authigenic clay mineral product-ion in ancient Martian lakes. Clay Clay Miner. 59, 339–358.
Caracciolo, L., 2020. Sediment generation and sediment routing systems from a quantitative provenance analysis perspective: review, application and future development. Earth Sci. Rev. 209, 103226.
Carvalho, A.S.G., Dani, N., De Ros, L.F., Zambonato, E.E., 2014. The impact of early diagenesis on the reservoir quality of pre-salt (aptian) sandstones in the Espirito Santo Basin, Eastern Brazil. J. Petrol. Geol. 37, 127–141.
Deconinck, J.F., Crasquin, S., Bruneau, L., Pellenard, P., Baudin, F., Feng, Q., 2014. Diagenesis of clay minerals and K-bentonites in late permian/early Triassic sediments of the Sichuan basin (chaotian section, Central China). J. Asian Earth Sci. 81, 28–37.
Folk, R.L., 1980. Petrology of Sedimentary Rocks. Hemphill Publishing, Austin, Texas, pp. 1–182.
Henares, S., Caracciolo, L., Cultrone, G., Fernández, J., Viseras, C., 2014. The role of diagenesis and depositional facies on pore system evolution in a Triassic outcrop analogue (SE Spain). Mar. Petrol. Geol. 51, 136–151.
Heydari, E., Wade, W.J., 2002. Massive recrystallization of low-Mg calcite at high temperatures in hydrocarbon source rocks: implications for organic acids as factors in diagenesis. AAPG Bull. 86, 1285–1303.
Jiang, Z., Liu, H., Zhang, S., Su, X., Jiang, Z., 2011. Sedimentary characteristics of largescale lacustrine beach-bars and their formation in the Eocene boxing sag of Bohai Bay Basin, east China. Sedimentology 58, 1087–1112.
Karim, A., Pe-Piper, G., Piper, D.J.W., 2010. Controls on diagenesis of lower cretaceous reservoir sandstones in the western sable subbasin, offshore Nova Scotia. Sediment. Geol. 224, 65–83.
Lampe, C., Song, G.Q., Cong, L.Z., Mu, X., 2012. Fault control on hydrocarbon migration and accumulation in the Tertiary Dongying depression, Bohai Basin, China. AAPG Bull. 96, 983–1000.
Liu, J., Wang, J., Cao, Y., Song, G., 2017. Sedimentation in a continental high-frequency oscillatory lake in an arid climatic background: a case study of the lower Eocene in the Dongying depression, China. J. Earth Sci. 28 (4), 628–644.
Ma, B., Cao, Y., Eriksson, K.A., Jia, Y., Wang, Y., 2016. Burial evolution of evaporites with implications for sublacustrine fan reservoir quality: a case study from the Eocene Es4x interval, Dongying depression, Bohai Bay Basin, China. Mar. Petrol. Geol. 76, 98–114.
MacDonald, A.J., Spooner, E.T.C., 1981. Calibration of a Linkam TH 600 programmable heating-cooling stage for microthermometric examination of fluid inclusions. Econ. Geol. 76, 1248–1258.
Mefteh, S., Medhioub, M., Essefi, E., Jamoussi, F., 2014. Effect of diagenesis on clay mineralogy and organic matter in the Tunisian southern subsurface. J. Geol. Soc. India 83, 198–210.
Meng, J., Liu, L., Jiang, Z., Wang, Y., Gao, Y., Liu, S., 2011. Geochemical characteristics of crude oil and oil-source correlation of the Paleogene "red bed" in the south slope of the dongying depression, Bohai Bay Basin, China. Energy Explor. Exploit. 29, 397–413.
Morad, S., Ketzer, J.M., De Ros, L.F., 2000. Spatial and temporal distribution of diagenetic alterations in siliciclastic rocks: implications for mass transfer in sedimentary basins. Sedimentology 47, 95–120.
Morad, S., Al-Ramadan, K., Ketzer, J.M., De Ros, L.F., 2010. The impact of diagenesis on the heterogeneity of sandstone reservoirs: a review of the role of depositional facies and sequence stratigraphy. AAPG Bull. 94, 1267–1309.
Nguyen, B.T.T., Jones, S.J., Goulty, N.R., Middleton, A.J., Grant, N., Ferguson, A., Bowen, L., 2013. The role of fluid pressure and diagenetic cements for porosity preservation in Triassic fluvial reservoirs of the Central Graben, North Sea. AAPG Bull. 97, 1273–1302.
Osborne, M.J., Swarbrick, R.E., 1999. Diagenesis in North Sea HPHT clastic reservoirs-consequences for porosity and overpressure prediction. Mar. Petrol. Geol. 16, 337–353.
Paytan, A., Gray, E.T., Ma, Z., Erhardt, A., Faul, K., 2011. Application of sulphur isotopes for stratigraphic correlation. Isot. Environ. Health Stud. 48, 195–206.
Qiu, N., Li, S., Zeng, J., 2004. Thermal history and tectonic-thermal evolution of the Jiyang depression in the Bohai Bay basin, east China. Acta Geol. Sin. 78, 263–269 (in Chinese with English abstract).
Rossi, C., Kalin, O., Arribas, J., Tortosa, A., 2002. Diagenesis, provenance and reservoir quality of triassic TAGI sandstones from ourhoud field, Berkine (Ghadames) basin, Algeria. Mar. Petrol. Geol. 19, 117–142.
Schmid, S., Worden, R.H., Fisher, Q.J., 2004. Diagenesis and reservoir quality of the Sherwood sandstone (Triassic), corrib field, Slyne basin, west of Ireland. Mar. Mar. Petrol. Geol. 21, 299–315.
Wang, J., Cao, Y., Liu, H., Gao, Y., 2015. Formation conditions and sedimentary model of over-flooding lake deltas within continental lake basins: an example from the Paleogene in the Jiyang Subbasin, Bohai Bay Basin. Acta Geol. Sin. Eng. Ed. 89 (1), 270–284.
Wang, J., Cao, Y., Liu, K., Liu, J., Xue, X., Xu, Q., 2016. Pore fluid evolution, distribution and water-rock interactions of carbonate cements in red-bed sandstone reservoirs in the Dongying Depression, China. Mar. Petrol. Geol. 72, 279–294.
Wang, J., Cao, Y., Song, G., Liu, H., 2017. Diagenetic evolution and formation mechanisms of high-quality reservoirs under multiple diagenetic environmental constraints: an example from the Paleogene beach-bar sandstone reservoirs in the Dongying depression, Bohai Bay basin. Acta Geol. Sin. Eng. Ed. 91 (1), 232–248.
Wang, J., Cao, Y., Liu, K., Costanzo, A., Feely, M., 2018. Diagenesis and evolution of the lower Eocene red-bed sandstone reservoirs in the Dongying Depression, China. Mar. Petrol. Geol. 94, 230–245.
Wang, J., Cao, Y., Liu, K., Wang, X., Xiao, J., Xie, N., 2019a. Mass transfer between mudstone-sandstone interbeds during diagenesis as revealed from the type and distribution of carbonate cements in the Eocene beach-bar sandstones, Bohai Bay Basin. Mar. Petrol. Geol. 110, 21–34.
Wang, J., Cao, Y., Xiao, J., Liu, K., Song, M., 2019b. Factors controlling reservoir properties and hydrocarbon accumulation of the Eocene lacustrine beach-bar sandsto-nes in the Dongying Depression, Bohai Bay Basin, China. Mar. Petrol. Geol. 99, 1–16.
Wilkinson, M.D., Haszeldine, R.S., Couples, G.D., 1997. Secondary porosity generation during deep burial associated with over-pressure leak-off: fulmar Formation, United Kingdom Central Graben. AAPG Bull. 81, 803–813.
Wilson, M.E.J., Wah, E.C.E., Dorobek, S., Lunt, P., 2013. Onshore to offshore trends in carbonate sequence development, diagenesis and reservoir quality across a land-attached shelf in SE Asia. Mar. Petrol. Geol. 45, 349–376.
Zhang, Y., Kaiser, K., Li, L., Zhang, D., Ran, Y., Benner, R., 2014. Sources, distributions, and early diagenesis of sedimentary organic matter in the Pearl River region of the South China Sea. Mar. Chem. 158, 39–48.